Interpretation of pile lateral response from deflection measurement data
A compressive sampling-based method

Zhao, Tengyuan; Wang, Yu

Published in:
Soils and Foundations

Published: 01/08/2018

Document Version:
Final Published version, also known as Publisher's PDF, Publisher's Final version or Version of Record

Published version (DOI):
10.1016/j.sandf.2018.05.002

Publication details:
Zhao, T., & Wang, Y. (2018). Interpretation of pile lateral response from deflection measurement data: A compressive sampling-based method. *Soils and Foundations*, *58*(4), 957-971. https://doi.org/10.1016/j.sandf.2018.05.002

HOSTED BY
ELSEVIER
Available online at www.sciencedirect.com
ScienceDirect
Soils and Foundations 58 (2018) 957–971
www.elsevier.com/locate/sandf

Interpretation of pile lateral response from deflection measurement data: A compressive sampling-based method

Tengyuan Zhao *, Yu Wang

Department of Architecture and Civil Engineering, City University of Hong Kong, Tat Chee Avenue, Kowloon, Hong Kong

Received 3 September 2017; received in revised form 28 April 2018; accepted 18 May 2018
Available online 28 June 2018

Abstract

The performance of piles under lateral loading, i.e., the lateral response of piles, may be evaluated by in situ lateral loading tests. Inclinometers are frequently installed along the pile depth to measure the pile lateral deflection during the loading tests. Other pile responses, such as the bending moment and shear force, may be further obtained through high-order differentiation of the deflection measurement data with respect to depth. As inclinometers measure the pile deflection at a number of pre-specified depths, the deflection measurement data are discrete. Performing high-order derivatives on discrete deflection data is tricky and sometimes provides misleading results, particularly when the pile response is nonlinear. This paper proposes an innovative approach for interpreting the lateral response of piles from discrete deflection measurement data. The proposed method is based on a new sampling theorem in digital signal processing called compressive sensing/sampling (CS). The method is illustrated using a real case history in the USA, and the results show that the proposed method can provide reasonable interpretations of the lateral response of piles. A sensitivity study is also carried out to systematically explore the performance of the proposed method.

Keywords: Pile lateral response; Compressive sensing (CS); Deflection data; Differentiation of discrete data

1. Introduction

Piles or drilled shafts are routinely used as deep foundations to deal with adverse soil conditions, such as highly compressible or expansive soils (e.g., Das, 2015; Gu et al., 2016; Gupta and Basu, 2017). They are also used to stabilize unstable slopes (e.g., Poulos, 1995; Hassiotis et al., 1997; Motamed et al., 2010; Kourkoulis et al., 2011, 2012; Sun et al., 2013). In such cases, the piles/drilled shafts may be subject to lateral loading, leading to horizontal displacement or deflections. The performance of piles under lateral loading may be evaluated by in situ lateral pile loading tests. Strain gauges and inclinometers are frequently installed along the pile depth to measure the pile response to lateral loading during the pile loading tests. Inclinometers directly measure the lateral deflection along the piles, and other pile responses can be conveniently derived from the deflection data (e.g., Brown et al., 1994; Lin et al., 2005). The lateral response interpreted from the deflection measurement data can be used as a supplement to, or as one means of "calibrating", the strain gauge data (e.g., Brown et al., 1994).

The pile lateral response of interest in engineering practice includes the distribution of bending moments (M) and shear forces (V) along the piles and the soil resistance per unit length of the piles (p) when they are subject to lateral loading. It should be noted that p has a unit of kN/m, and it represents the horizontal soil resistance per unit length of depth. In accordance with the beam theory, M, V, and

Peer review under responsibility of The Japanese Geotechnical Society.
* Corresponding author.
E-mail addresses: tengyzhao2@cityu.edu.hk (T. Zhao), yuwang@cityu.edu.hk (Y. Wang).

https://doi.org/10.1016/j.sandf.2018.05.002
0038-0806/

p can be readily derived from the lateral deflection measurement data, y, which are expressed as follows (e.g., Hetenyi, 1946; McClelland and Focht, 1958):

$$M = EI\frac{d^2y}{dz^2} \tag{1}$$

$$V = EI\frac{d^3y}{dz^3} = \frac{dM}{dz} \tag{2}$$

$$p = EI\frac{d^4y}{dz^4} = \frac{dV}{dz} \tag{3}$$

where z = depth along the piles, E = elastic modulus of the piles, and I = moment inertia of the piles. EI is the flexural rigidity. d^2y/dz^2, d^3y/dz^3, and d^4y/dz^4 are the second-, third- and fourth-order derivatives of y with respect to depth z, respectively. Using the p values obtained from Eq. (3) and their corresponding y values, p-y curves may also be obtained.

Since inclinometers measure the pile deflection at a number of pre-specified depths, the deflection measurement data are discrete data. It is not a trivial task to calculate the derivatives of discrete data y with respect to z, i.e., d^2y/dz^2, d^3y/dz^3, and d^4y/dz^4 in Eqs. (1)–(3), respectively. To properly obtain these high-order derivatives, several methods have been developed in geotechnical literature. For example, Brown et al. (1994) proposed the use of a least-squares regression to interpret the deflection measurement data, followed by the calculation of derivatives using the finite difference code COM624 (Wang and Reese, 1991). This method minimizes the difference between the measured and the computed deflection data, which are calculated from a predetermined analytical p-y model in COM624 (Wang and Reese, 1991). However, the mathematical function form of the p-y curves must be predetermined, and this predetermined function form may affect the obtained pile response. In addition, iteration is required for several soil parameters in order to calibrate the p-y curves with this method. Lin et al. (2005), Lin and Liao (2006), and Chien et al. (2013) utilized the concept of energy conservation within a pile-soil system. Based on this concept, Fourier series functions are used to represent the deflection measurement data. In addition, the Cesaro sum technique (Hardy, 2000) was adopted in their studies to guarantee the convergence of the series after differentiation. However, because of the requirement of energy conservation in their method, it is more suitable for long piles/drilled shafts than for short ones. For short piles/drilled shafts, modification needs to be carried out on the strain energy and the potential energy used in their method (Lin and Liao, 2006; Lin et al., 2010). Yamin and Liang (2010) proposed interpreting the lateral response of shafts using the principle of superposition (i.e., the shaft deflection at a depth due to the superposition of the lateral load equals the sum of the shaft deflections by individual lateral loads applied at that depth). Unfortunately, their method is only applicable when the piles/drilled shafts respond in a linear elastic range, which is not necessarily the case in engineering practice. Brandenberg et al. (2010) also presented a numerical differentiation technique, i.e., the weighted residual method (e.g., Wilson, 1998; Wilson et al., 2000), to recursively calculate the derivatives of the discrete measurement data. However, their technique cannot calculate the derivatives at locations where deflection data have not been measured. Other methods were also developed to interpret the lateral response of piles, such as the polynomial fitting of the deflection measurements (e.g., Ooi and Ramsey, 2003) and the finite element/difference method (e.g., Yang and Jeremić, 2002; Karthigeyan et al., 2007; Martin and Chen, 2005). However, it is generally not easy to determine the most appropriate order for the polynomial fitting of the measurement data (e.g., Wang et al., 2017). On the other hand, finite element/difference methods require detailed site information (e.g., soil layer thickness) and soil properties. It is difficult, therefore, to evaluate the pile lateral responses from the deflection measurement data for sites without detailed site information or soil properties.

This paper proposes a new method for interpreting the lateral response of piles/drilled shafts under lateral loading, which is able to bypass the above-mentioned problems. The proposed method is based on a novel sampling theorem in digital signal processing called compressive/compressed sensing/sampling (CS) (e.g., Candès et al., 2006; Donoho, 2006; Candès and Wakin, 2008). It requires only discrete deflection measurement data y and EI (See Eqs. (1)–(3)) as input, and returns the distribution of bending moments, M (Eq. (1)), shear forces, V (Eq. (2)), and soil resistance, p (Eq. (3)) along depth as output. Moreover, input y might be measured with unequal intervals, while output M, V, and p can be almost continuous with a high resolution, and they can be obtained at locations where no deflection data have been measured. In this paper, the CS theory is firstly reviewed, followed by an explanation of the development of the proposed method. Then, a real case study is adopted to illustrate the proposed approach. A sensitivity study is also performed to further validate the capability of the proposed method.

2. Compressive sampling

2.1. Framework

Compressive/compressed sensing/sampling (CS) is a novel sampling theorem which can reconstruct complete information on a signal from partial information on it (e.g., Candès et al., 2006; Donoho, 2006; Candès and Wakin, 2008; Foucart and Rauhut, 2013; Huang et al., 2014). A signal is defined as the variation of a quantity with time or space, such as the variation in the lateral deflection along piles. CS relies on the fact that many natural signals are compressible. The term "compressible" means that a real-valued signal $\boldsymbol{f}$ can be concisely represented by a weighted summation of only several basis functions (e.g., orthogonal cosine functions). $\boldsymbol{f}$ is a column vector with a

length of N. Mathematically, $\boldsymbol{f}$ is expressed as follows (e.g., Candès and Wakin, 2008; Wang et al., 2018; Zhao and Wang, 2018):

$$\boldsymbol{f} = \sum_{i=1}^{N} \mathbf{B}_i \omega_i = \mathbf{B}\boldsymbol{\omega} \tag{4}$$

where $\boldsymbol{B}_i$ represents the i-th column of orthonormal matrix $\mathbf{B}$ in Eq. (4), and each column of $\mathbf{B}$ represents a basis function (e.g., cosine function) which is independent of $\boldsymbol{f}$. ω_i represents the i-th element in column vector $\boldsymbol{\omega}$ and the weight corresponding to $\boldsymbol{B}_i$. Matrix $\mathbf{B}$ can be constructed readily using a Fourier transform (e.g., Oppenheim and Schafer, 1989), a wavelet transform (e.g., Daubechies, 1992; Mallat, 1999) or a discrete cosine transform (e.g., Salomon, 2004), which will be used here. In this study, an upright bold letter is used to denote a matrix, while an italic bold symbol is used to denote a column vector. Due to the compressibility of $\boldsymbol{f}$, most elements of $\boldsymbol{\omega}$ are almost zero (e.g., Candès and Wakin, 2008). In the context of CS, the several non-trivial elements (i.e., elements with significantly large magnitudes) of $\boldsymbol{\omega}$ can be identified and estimated using the limited measurement data on $\boldsymbol{f}$, i.e., $\boldsymbol{y}$, where $\boldsymbol{y}$ is a column vector with a length of K ($K \ll N$). Mathematically, the relation between $\boldsymbol{y}$ and $\boldsymbol{\omega}$ is expressed as

$$\mathbf{y} = \boldsymbol{\Psi}\boldsymbol{f} = \boldsymbol{\Psi}\mathbf{B}\boldsymbol{\omega} = \mathbf{A}\boldsymbol{\omega} = \sum_{i=1}^{N} \boldsymbol{A}_i \omega_i \tag{5}$$

where $\mathbf{A} = \boldsymbol{\Psi}\mathbf{B}$ is a matrix with the dimensions of $K \times N$; $\boldsymbol{\Psi}$ represents the locations of the components of $\boldsymbol{y}$ in $\boldsymbol{f}$, and it is also a matrix with the dimensions of $K \times N$. The construction of $\boldsymbol{\Psi}$ can be found in Wang and Zhao (2016, 2017) and Zhao et al. (2018). Since $K \ll N$, Eq. (5) is underdetermined. However, due to the compressibility of $\boldsymbol{\omega}$ (i.e., most components of $\boldsymbol{\omega}$ are almost zero), Eq. (5) can be solved using some algorithms, such as the orthogonal matching pursuit algorithm (e.g., Pati et al., 1993; Tropp and Gilbert, 2007), as will be described in the next subsection. Once the non-trivial components in $\boldsymbol{\omega}$ have been identified and estimated, $\boldsymbol{f}$ can be approximated as $\hat{\boldsymbol{f}}$, which is expressed as

$$\hat{\boldsymbol{f}} = \mathbf{B}_s \omega_s \tag{6}$$

where $\boldsymbol{\omega}_s$ and $\mathbf{B}_s$ represent the S non-trivial components in $\boldsymbol{\omega}$ and the corresponding columns in $\mathbf{B}$, respectively. $\mathbf{B}_s$ is a matrix with the dimensions of $N \times S$ and $\boldsymbol{\omega}_s$ is a column vector with a length of S. To identify and estimate the non-trivial elements in $\boldsymbol{\omega}$ from Eq. (5), the orthogonal matching pursuit (OMP) algorithm is used, as discussed below.

2.2. Orthogonal matching pursuit (OMP)

As implied in Eq. (5), $\boldsymbol{y}$ can be considered as a weighted summation of columns $\boldsymbol{A}_i$, and ω_i represents the weight corresponding to $\boldsymbol{A}_i$. As $\boldsymbol{A}_i$ is at least approximately orthogonal to $\boldsymbol{A}_j$ (i.e., the dot product between $\boldsymbol{A}_i$ and $\boldsymbol{A}_j$ is nearly zero if $i \neq j$), the contribution of $\boldsymbol{A}_i$ to $\boldsymbol{y}$ can be considered as independent of each other (e.g., Pati et al., 1993). The more $\boldsymbol{A}_i$ contributes to $\boldsymbol{y}$, the more $\boldsymbol{y}$ is similar to $\boldsymbol{A}_i$. The OMP algorithm utilizes this property to iteratively select the non-trivial columns in $\mathbf{A}$ and to estimate the corresponding weight by the least-squares method. The procedure is briefly summarized below (e.g., Pati et al., 1993; Wang and Zhao, 2016).

(1) Define initial residual $\boldsymbol{r}_t$ as $\boldsymbol{r}_t = \boldsymbol{y}$. Set index set Ω_t as an empty set. Ω_t shall record the location of the columns of $\mathbf{A}$ corresponding to $\boldsymbol{\omega}_s$. Subscript "t" in this study represents the iteration step; it is initially set as $t = 0$.
(2) Calculate the similarity of $\boldsymbol{r}_t$ with each column of $\mathbf{A}$, i.e., $\lambda_i = \left| \frac{\boldsymbol{r}_t^T \boldsymbol{A}_i}{\sqrt{\boldsymbol{r}_t^T \boldsymbol{r}_t}\sqrt{\boldsymbol{A}_i{}^T \boldsymbol{A}_i}} \right| (i = 1, 2, \ldots, N)$. Find the maximum λ within λ_i ($i = 1, 2, \ldots, N$) and record the corresponding index in Ω_t.
(3) Select the column in $\mathbf{A}$ corresponding to the maximum λ, and append it to matrix $\mathbf{A}_{s,t}$, which has the dimensions of $K \times S$. Set the columns selected in $\mathbf{A}$ to zero.
(4) Estimate $\boldsymbol{\omega}_s$ by the least squares method as $\boldsymbol{\omega}_{s,t} = [(\mathbf{A}_{s,t})^T \mathbf{A}_{s,t}]^{-1} (\mathbf{A}_{s,t})^T \boldsymbol{y}$.
(5) Estimate the best-fitted measurement data as $\hat{\boldsymbol{y}} = \mathbf{A}_{s,t} \boldsymbol{\omega}_{s,t}$ and update the residual $\boldsymbol{r}_{t+1} = \boldsymbol{r}_t - \hat{\boldsymbol{y}}$.
(6) Repeat Steps (2)–(5) until the relative error between $\boldsymbol{y}$ and $\hat{\boldsymbol{y}}$, i.e., $\varepsilon = \sqrt{\sum_{i=1}^{K} (\hat{y}_i - y_i)^2} / \sqrt{\sum_{i=1}^{K} (y_i)^2}$, is relatively small, such as $\varepsilon \leq 0.05$.

It is worthwhile to note that measurement data $\boldsymbol{y}$ may be measured with unequal intervals. Furthermore, although $\boldsymbol{y}$ only has a length of K, reconstructed signal $\hat{\boldsymbol{f}}$ has a length of N. Since $\hat{\boldsymbol{f}}$ is explicitly represented by a weighted summation of S basis functions (e.g., cosine functions in this study), derivatives of $\hat{\boldsymbol{f}}$ can be obtained analytically, as will be shown in the next section.

3. Differentiation of discrete deflection measurement data

3.1. Derivatives

The deflection data of piles/drilled shafts vary with depth. Therefore, the deflection data can be considered as signals. In such cases, the CS theory can be used to reconstruct a high-resolution pile deflection profile, $\hat{\boldsymbol{f}}$, from discrete deflection data $\boldsymbol{y}$ measured by inclinometers set at either equal or unequal intervals. The discrete cosine transform (DCT) is used to construct $\mathbf{B}$ in this study, and the basis functions used in the DCT are cosine functions. Therefore, $\hat{\boldsymbol{f}}$ can be represented by a weighted summation of several cosine functions and has an analytical expression. It should be noted that each column $\boldsymbol{B}_j$ in $\mathbf{B}$ corresponds to a

cosine function, and that the elements in $\boldsymbol{B}_j$ are expressed as Eq. (7) (e.g., Salomon, 2004):

$$\mathrm{B}_{i,j} = c_j \cos\left(\frac{(\mathrm{j}-1)(\mathrm{i}-0.5)\pi}{\mathrm{N}}\right) \tag{7}$$

where $\mathrm{B}_{i,j}$ represents the i-th element of column $\boldsymbol{B}_j$. $c_j = \begin{cases} \sqrt{1/N} & for\ j = 1 \\ \sqrt{2/N} & otherwise \end{cases}$ is a normalizing constant which guarantees that matrix $\mathbf{B}$ is an orthonormal matrix. Index i in $\mathrm{B}_{i,j}$ is related to the pile depth, which is expressed as $i = (z_i - z_1)/\eta + 1$. z_1 and z_i correspond to the depths of the first and i-th point of $\hat{\boldsymbol{f}}$, respectively, and η represents a resolution that engineers like to have in reconstructed deflection data $\hat{\boldsymbol{f}}$. Substituting $i = (z_i - z_1)/\eta + 1$ into Eq. (7) and rearranging the equation lead to the expression of $\mathrm{B}_{i,j}$ in terms of pile depths.

$$B_{i,j} = c_j \cos\left(2\pi\left(\frac{(\mathrm{j}-1)(\mathrm{z_i}-\mathrm{z_1})}{2\mathrm{N}\eta} + \frac{\mathrm{j}-1}{4\mathrm{N}}\right)\right) \tag{8}$$

Therefore, $\hat{\boldsymbol{f}}$ can also be expressed as a function of the pile depths, and the i-th element of $\hat{\boldsymbol{f}}$, i.e., $\hat{f}_i$, can be expressed as Eq. (9) in accordance with Eq. (6).

$$\begin{aligned}\hat{f}_i &= \sum_{j=1}^{S} B_{i,j}\omega_{s_j} \\ &= \sum_{j=1}^{S} \omega_{s_j} c_j \cos\left(2\pi\left(\frac{(\mathrm{j}-1)(\mathrm{z_i}-\mathrm{z_1})}{2\mathrm{N}\eta} + \frac{\mathrm{j}-1}{4\mathrm{N}}\right)\right)\end{aligned} \tag{9}$$

where ω_{s_j} represents the j-th element of $\boldsymbol{\omega}_s$.

As reconstructed deflection data $\hat{\boldsymbol{f}}$ is explicitly represented as a function of pile depth, the derivatives of $\hat{\boldsymbol{f}}$ with depth can be obtained analytically. The second-, third-, and fourth-order derivatives of $\hat{\boldsymbol{f}}$, with respect to depth z_i, are shown in Eqs. (10)–(12), respectively, as follows:

$$\begin{aligned}\frac{d^2\hat{f}_i}{dz_i^2} &= \sum_{j=1}^{S} \omega_{s_j} \frac{d^2 B_{i,j}}{dz_i^2} \\ &= -\sum_{j=1}^{S} \omega_{s_j} c_j \left(\pi\frac{(j-1)}{N\eta}\right)^2 \cos\left(2\pi\left(\frac{(\mathrm{j}-1)(\mathrm{z_i}-\mathrm{z_1})}{2\mathrm{N}\eta} + \frac{\mathrm{j}-1}{4\mathrm{N}}\right)\right)\end{aligned} \tag{10}$$

$$\begin{aligned}\frac{d^3\hat{f}_i}{dz_i^3} &= \sum_{j=1}^{S} \omega_{s_j} \frac{d^3 B_{i,j}}{dz_i^3} \\ &= \sum_{j=1}^{S} \omega_{s_j} c_j \left(\pi\frac{(j-1)}{N\eta}\right)^3 \sin\left(2\pi\left(\frac{(\mathrm{j}-1)(\mathrm{z_i}-\mathrm{z_1})}{2\mathrm{N}\eta} + \frac{\mathrm{j}-1}{4\mathrm{N}}\right)\right)\end{aligned} \tag{11}$$

$$\begin{aligned}\frac{d^4\hat{f}_i}{dz_i^4} &= \sum_{j=1}^{S} \omega_{s_j} \frac{d^4 B_{i,j}}{dz_i^4} \\ &= \sum_{j=1}^{S} \omega_{s_j} c_j \left(\pi\frac{(j-1)}{N\eta}\right)^4 \cos\left(2\pi\left(\frac{(\mathrm{j}-1)(\mathrm{z_i}-\mathrm{z_1})}{2\mathrm{N}\eta} + \frac{\mathrm{j}-1}{4\mathrm{N}}\right)\right)\end{aligned} \tag{12}$$

where $\frac{d^2\hat{f}_i}{dz_i^2}$, $\frac{d^3\hat{f}_i}{dz_i^3}$, and $\frac{d^4\hat{f}_i}{dz_i^4}$ represent the second-, third-, and fourth-order derivatives of $\hat{\boldsymbol{f}}$, respectively, at depth z_i. Then, substituting Eqs. (10)–(12) into Eqs. (1)–(3), respectively, leads to the bending moment (M), shear force (V), and soil resistance per unit length (p) at depth z_i.

Although $\hat{\boldsymbol{f}}$ can be reconstructed and represented efficiently by the cosine functions, the derivatives of $\hat{\boldsymbol{f}}$ might exhibit significant and unrealistic fluctuations, especially at the top and bottom of the piles. Since the top and bottom of the piles are two boundaries of the reconstructed $\hat{\boldsymbol{f}}$, it is mathematically problematic to perform derivatives at the boundaries due to the continuity condition. To avoid this problem and to improve the performance of the proposed method, the pre-processing of the deflection measurement data is proposed in this study to create a periodic signal (e.g., Li et al., 1998; Wang and O'Rourke, 2007) that satisfies the continuity condition at the top and bottom of the piles, as will be described in the next subsection.

3.2. Pre-processing of deflection measurement data

As shown in Fig. 1, the measured deflection data $\boldsymbol{y}$ in Fig. 1(a) is decomposed into two components, namely, a linear component, $\boldsymbol{y}_L$, seen in Fig. 1(b), and a nonlinear component, $\boldsymbol{y}_{NL}$, seen in Fig. 1(c), and $\boldsymbol{y} = \boldsymbol{y}_L + \boldsymbol{y}_{NL}$. Linear component $\boldsymbol{y}_L$ may be represented analytically and conveniently by a linear function, the derivatives of which can be easily obtained analytically. The nonlinear component will be transformed into a periodic signal to improve the smoothness and the continuity of the measurement data. Then, the proposed CS-based method will be applied to reconstruct the periodic signal and to perform high-order derivatives of the reconstructed periodic signal.

The linear function representing linear component $\boldsymbol{y}_L$ can be expressed as

$$y_L = az + b \tag{13}$$

where a and b represent the slope and the intercept, respectively, of the linear function defined by the first and last points of $\boldsymbol{y}$, i.e., y_1 and y_K. $a = (y_1 - y_K)/(z_1 - z_K)$ and $b = y_1 - a \times z_K$; z_K represents the depth corresponding to y_K. Eq. (13) shall be used only when reconstructing the linear component of $\hat{\boldsymbol{f}}$, i.e., $\hat{\boldsymbol{f}}_L$. The nonlinear component of $\hat{\boldsymbol{f}}$, i.e., $\hat{\boldsymbol{f}}_{NL}$, shall be reconstructed using nonlinear component $\boldsymbol{y}_{NL}$.

Using nonlinear component $\boldsymbol{y}_{NL}$, a periodic signal, $\boldsymbol{y}_P$, is generated by alternately cloning the $\boldsymbol{y}_{NL}$ itself and its

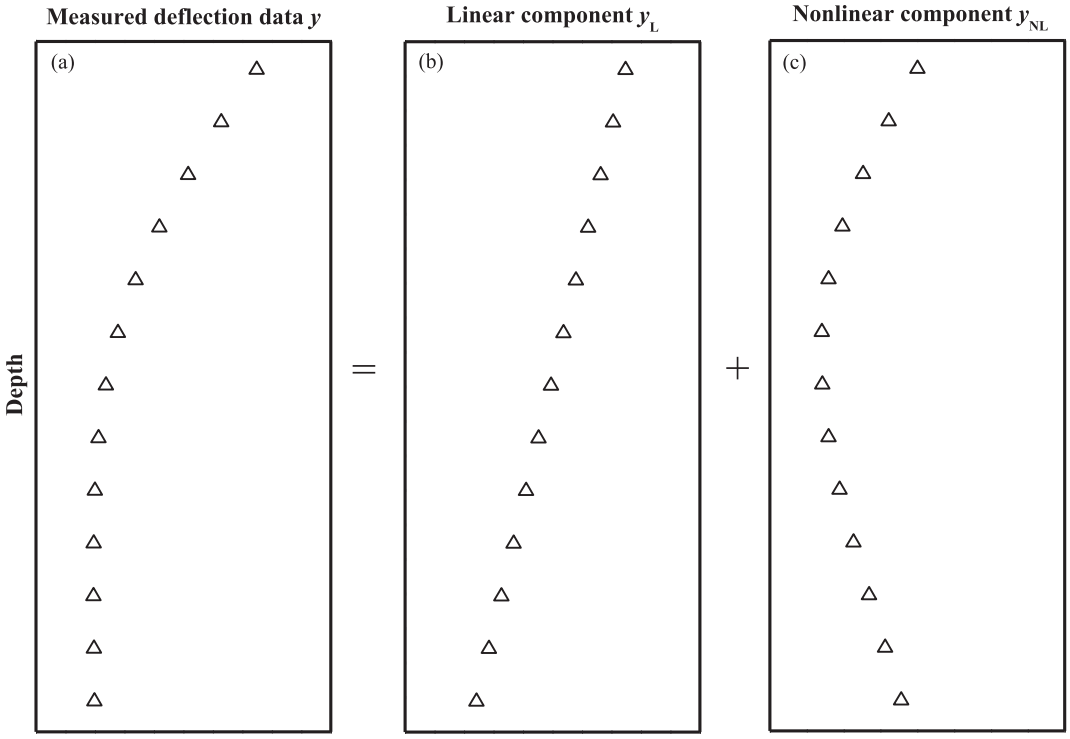

Fig. 1. Decomposition of deflection measurement data from lateral pile loading tests.

folded and inverted copies along the depth coordinates, as shown in Fig. 2(a) and (b). In such a way, the continuity condition at the top and bottom of the piles is improved. Subsequently, following the reconstruction procedure described in the previous section, this set of periodic measurement data $\boldsymbol{y_P}$ (illustrated in Fig. 2(b)) will be used as input for reconstructing the nonlinear component of $\hat{\boldsymbol{f}}$, i.e., $\hat{\boldsymbol{f}}_{\boldsymbol{NL}}$. Then, the derivatives described in the previous subsection can be obtained. It should be noted that only the reconstructed deflection data together with their derivatives within the original pile depth are of real interest.

Using $\hat{\boldsymbol{f}}_{\boldsymbol{L}}$ and $\hat{\boldsymbol{f}}_{\boldsymbol{NL}}$ (note that $\hat{\boldsymbol{f}} = \hat{\boldsymbol{f}}_{\boldsymbol{L}} + \hat{\boldsymbol{f}}_{\boldsymbol{NL}}$) and Eqs. (10)–(12), the bending moment (M), shear force (V), and soil resistance (p) at depth z_i, can be rewritten as follows:

$$M_i = EI\frac{d^2\hat{f}_i}{dz_i^2} = EI\frac{d^2\left(\hat{f}_{L_i} + \hat{f}_{NL_i}\right)}{dz_i^2} = EI\frac{d^2\hat{f}_{NL_i}}{dz_i^2} \tag{14}$$

$$V_i = EI\frac{d^3\hat{f}}{dz_i^3} = EI\frac{d^3\left(\hat{f}_{L_i} + \hat{f}_{NL_i}\right)}{dz_i^3} = EI\frac{d^3\hat{f}_{NL_i}}{dz_i^3} = \frac{dM_i}{dz_i} \tag{15}$$

$$p_i = EI\frac{d^4\hat{f}}{dz_i^4} = EI\frac{d^4\left(\hat{f}_{L_i} + \hat{f}_{NL_i}\right)}{dz_i^4} = EI\frac{d^4\hat{f}_{NL_i}}{dz_i^4} = \frac{dV_i}{dz_i} \tag{16}$$

where $\hat{f}_{L_i}$ and $\hat{f}_{NL_i}$ represent the i-th element of $\hat{\boldsymbol{f}}_{\boldsymbol{L}}$ and $\hat{\boldsymbol{f}}_{\boldsymbol{NL}}$, respectively. The high-order derivatives of the linear function are zero; therefore, terms $d^2\hat{f}_{L_i}/dz_i^2$, $d^3\hat{f}_{L_i}/dz_i^3$, and $d^4\hat{f}_{L_i}/dz_i^4$ in Eqs. (14)–(16), respectively, become zero.

It should be noted that the method proposed in this paper is for interpolating the measurement data at unobserved locations and for performing high-order derivatives on the interpolation results. It cannot be used for extrapolating the measurement data (i.e., providing results out of the measurement range). This interpolation nature of the proposed method is particularly suitable for inclinometer data, because inclinometers usually measure the lateral deflection from a point very close to the pile head to the pile bottom. In addition, it should be clarified that the pre-processing procedure for generating a periodic signal is a commonly-used procedure in digital signal processing (e.g., Smith and Eddins, 1990; Boggess and Narcowich, 2009). The reason for using a periodic signal is that, when the measurement data are cloned to produce a periodic signal, many sets of original measurement data can be repeatedly used to improve the interpolation results, particularly at the head and bottom of a pile. The effect of the pre-processing procedure will be illustrated later in Section 5.3 of this paper.

It is worth noting that the method proposed in this study is focused on the derivatives of discrete measurement data $\boldsymbol{y}$, and that a constant EI (in Eqs. (14)–(16)) is used in this paper. However, the nonlinear moment-curvature behavior of a drilled shaft can be readily taken into account by replacing constant elastic modulus E with an effective elastic modulus when a drilled shaft exhibits highly nonlinear moment-curvature behavior. A detailed description of the effective elastic modulus is given in the literature (e.g., Reese and Van Impe, 2001; Ooi and Ramsey, 2003; Lin and Liao, 2006). In the next subsection, an implementation procedure will be briefly summarized for clear reference.

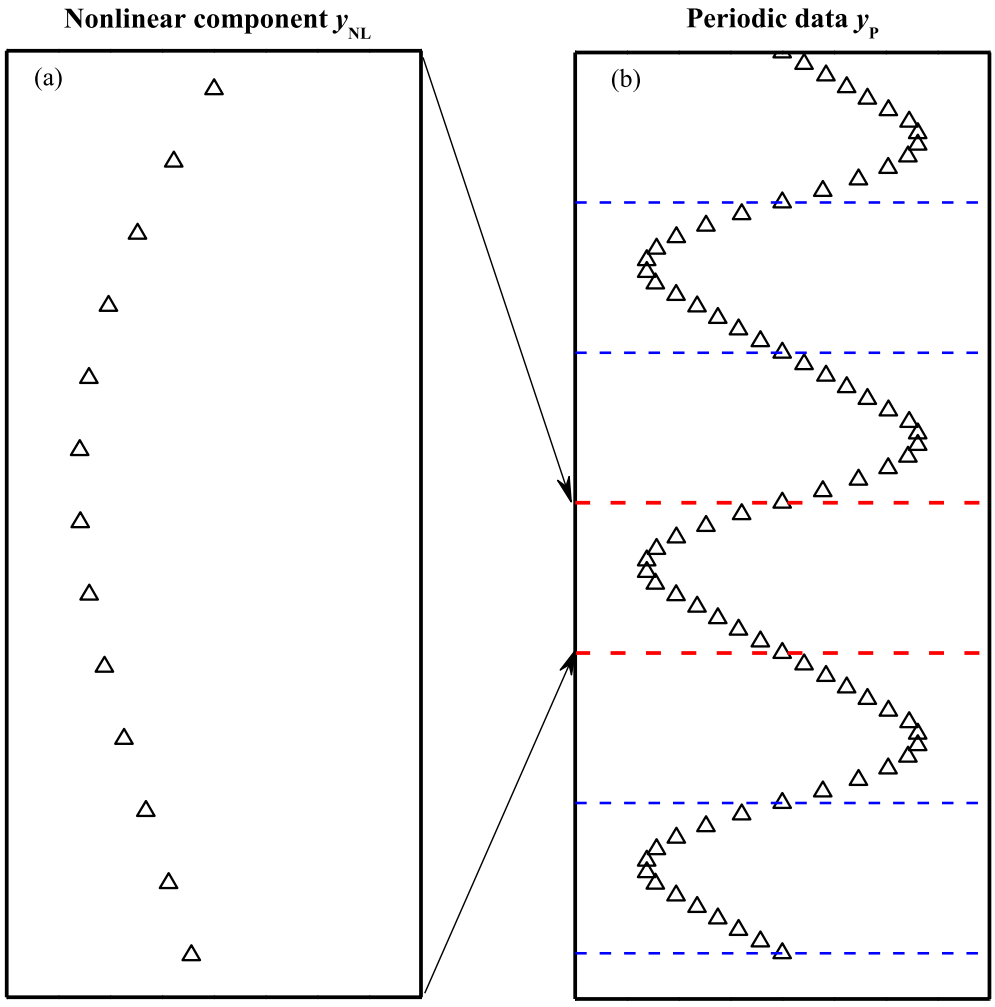

Fig. 2. Transformation from set of non-periodic data to set of periodic data for nonlinear component of measured data.

3.3. Implementation procedure

In this subsection, key steps and the associated equations of the proposed approach are summarized.

Step 1: Obtain deflection measurement data $\boldsymbol{y}$ versus depth and its length K. $\boldsymbol{y}$ can be measured with either equal or unequal intervals. The pile length for the deflection data of interest is h.
Step 2: Decompose $\boldsymbol{y}$ into two components, namely, linear component $\boldsymbol{y_L}$ and nonlinear component $\boldsymbol{y_{NL}}$.
Step 3: Derive the linear function of $\boldsymbol{y_L}$ (i.e., Eq. (13)) using the first and last points of $\boldsymbol{y}$ and their corresponding depths. Transform nonlinear component $\boldsymbol{y_{NL}}$ into a set of periodic deflection data $\boldsymbol{y_P}$ by cloning it and its folded and inverted copies (see Fig. 2(b)).
Step 4: Specify an interval η of interest. Note that η reflects the resolution that an engineer would like to have in $\hat{\boldsymbol{f}}$. Calculate the length of $\hat{\boldsymbol{f}}$ as $N = h/\eta+1$. When $\boldsymbol{y_{NL}}$ is transformed into a set of periodic data $\boldsymbol{y_P}$ by cloning it and its folded and inverted copies for L_P times, $\boldsymbol{y_P}$ would have a length of $K_P = 2L_PK - 2L_P + 1$. The reconstructed nonlinear component $\hat{\boldsymbol{f}}_P$ from $\boldsymbol{y_P}$ has a length of $N_P = 2L_PN - 2L_P + 1$.
Step 5: Construct matrix $\mathbf{B}$ with the dimensions of $N_P \times N_P$ using Eq. (7). Subsequently, construct matrices $\boldsymbol{\Psi}$ and $\mathbf{A} = \boldsymbol{\Psi}\mathbf{B}$, using the locations of $\boldsymbol{y_P}$.
Step 6: Determine the locations and values of the non-trivial coefficients in $\boldsymbol{\omega}$ using the OMP algorithm presented in previous section.
Step 7: Express deflection function $\hat{\boldsymbol{f}}_{\boldsymbol{P}}$ using Eq. (6), and calculate the second-, third-, and fourth-order derivatives of $\hat{\boldsymbol{f}}_{\boldsymbol{P}}$ with respect to depth, using Eqs. (10)–(12), respectively. Finally, substitute the derivatives of interest (i.e., the derivatives within the original pile length) into Eqs. (1)–(3), and the bending moment (M), the shear force (V) along the depths, and soil resistance (p) per unit length can be obtained along the pile length (see Eqs. (14)–(16)).

Although the proposed method involves many equations and a pre-processing procedure, it can be readily programmed as a user function or a toolbox using

computer software, such as MATLAB (Mathworks, 2017) in practice. In such cases, its execution is rather simple and straightforward. For illustration, the proposed method and procedure are used to derive the lateral response of piles using a case history in the USA.

4. Illustrative example

In this section, the proposed method is applied to derive the lateral response of a full-scale laterally loaded pile group at Salt Lake International Airport, Utah, USA (Rollins et al., 1998). This site consists of a layer of gravel fill from the ground surface to a depth of around 1.78 m, followed by a thin silt/sand layer with a thickness of around 0.42 m. From a depth of 2.2 m to 7.4 m, it is soft to medium-stiff clay and underlain by sandy silt and silty sand or silt (Rollins et al., 1998). In this pile load test, a group of 3 × 3 steel pipe piles was used, with a nominal center-to-center spacing of around 0.93 m. The layout of the 9 piles is illustrated in Fig. 3. It should be noted that all the pipe piles are closed-ended with an inner diameter of 0.305 m. The wall is 9.5 mm in thickness. After the piles were driven into the ground, the pile was in-filled with concrete. It was reported in Rollins et al. (1998) that the elastic modulus of the steel and concrete were 200 GPa and 17.5 GPa, respectively. In addition, the minimum yield stress of the steel was 331 MPa, while the compressive strength of the concrete was 20.7 MPa (Rollins et al., 1998). Both strain gauges and inclinometers were installed in this test. Therefore, both deflection data (from the inclinometers) and strain gauge data were available. However, only the deflection measurement data versus depth are used as input for the proposed method to derive the lateral response. The bending moment derived from the strain gauge data will be used for validation and comparison purposes only. It should be noted that deflection measurement data from inclinometers unavoidably contain measurement errors, which affect the interpretation results of the proposed method. Generally speaking, before the proposed method is used to interpret the lateral response, the measurement errors should firstly be excluded from the deflection measurement data or the measurement errors in the deflection measurement data should be considered as within an acceptable range.

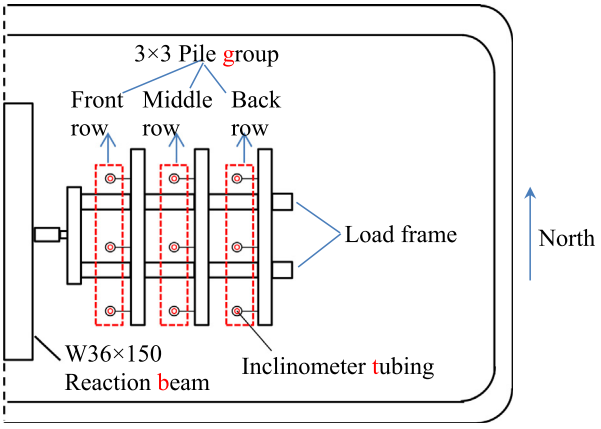

Fig. 3. Illustration of layout of 3 × 3 pipe pile test at Salt Lake International Airport (after Rollins et al., 1998).

In the tests, each row of piles was subject to lateral loading at the pile head, which was around 0.4 m above the ground surface. In this section, three different loading cases, namely, 97.9 kN/per pile (Case I), 66.7 kN/per pile (Case II), and 35.6 kN/per pile (Case III), were used to illustrate the proposed method. Correspondingly, different deflection data were measured with equal intervals of around 0.61 m for the three rows of piles, i.e., the front row, the middle row, and the back row. Fig. 4(a) plots $K = 14$ deflection measurement data for each of the three cases for the front row of piles by different symbols: open triangles for Case I, open squares for Case II, and open circles for Case III. The deflection data for these three cases are digitalized from Rollins et al. (1998).

Consider, for example, the deflection data of Case II for the front row (i.e., the open squares in Fig. 4(a)). The distance between the first and last points of the deflection measurement data is $h = 7.93$ m (Step 1). Then, this set of measured discrete deflection data is decomposed into two components, a linear component and a nonlinear component, as illustrated in Fig. 1 (Step 2). The linear component can be represented by a straight line, with a function of $y_L = -3.37z + 27.54$ $(0.25\text{ m} \le z \le 8.18\text{ m})$, using the first and last deflection measurement points, while the nonlinear component is transformed into a periodic function by alternately cloning itself and its folded and inverted copies along the depth coordinate for $L_P = 13$ times (the method for determining the L_P value will be shown in the next section), as illustrated in Fig. 2(a) and (b) (Step 3). The periodic data, $\boldsymbol{y_P}$, has a length of $K_P = 2L_PK\text{-}2L_P + 1 = 339$. Subsequently, an interval of interest, such as $\eta = 0.305$ m, is specified in this example, and $N = h/\eta + 1 = 27$. The reconstructed $\hat{\boldsymbol{f}}_{\boldsymbol{P}}$ (i.e., the nonlinear component directly reconstructed from $\boldsymbol{y_P}$) has a length of $N_P = 2L_PN\text{-}2L_P + 1 = 677$ (Step 4). Matrix $\mathbf{B}$ is constructed with the dimensions of $N_P \times N_P$, while matrix $\boldsymbol{\Psi}$ is constructed using the locations of $\boldsymbol{y_P}$. $\mathbf{A} = \boldsymbol{\Psi}\mathbf{B}$ (Step 5). Then, the locations and values of the non-trivial coefficients in $\boldsymbol{\omega}$ are determined using the OMP algorithm presented in the section entitled "Compressive sampling" (Step 6). Finally, $\hat{\boldsymbol{f}}_P$ is represented as the weighted summation of the cosine functions. High-order derivatives of interest, i.e., the derivatives within the original pile length, as shown in Fig. 2(b), can be obtained readily using Eqs. (10)–(12) (Step 7). Substituting the derivatives of interest into Eqs. (1)–(3) leads to the distribution of bending moments, shear forces, and soil resistance, as shown in Eqs. (14)–(16).

Adding the reconstructed nonlinear component within the original pile length to the linear function, i.e., $y_L = -3.37z + 27.54$, leads to the reconstructed deflection data along with the pile length with an interval of $\eta = 0.305$,

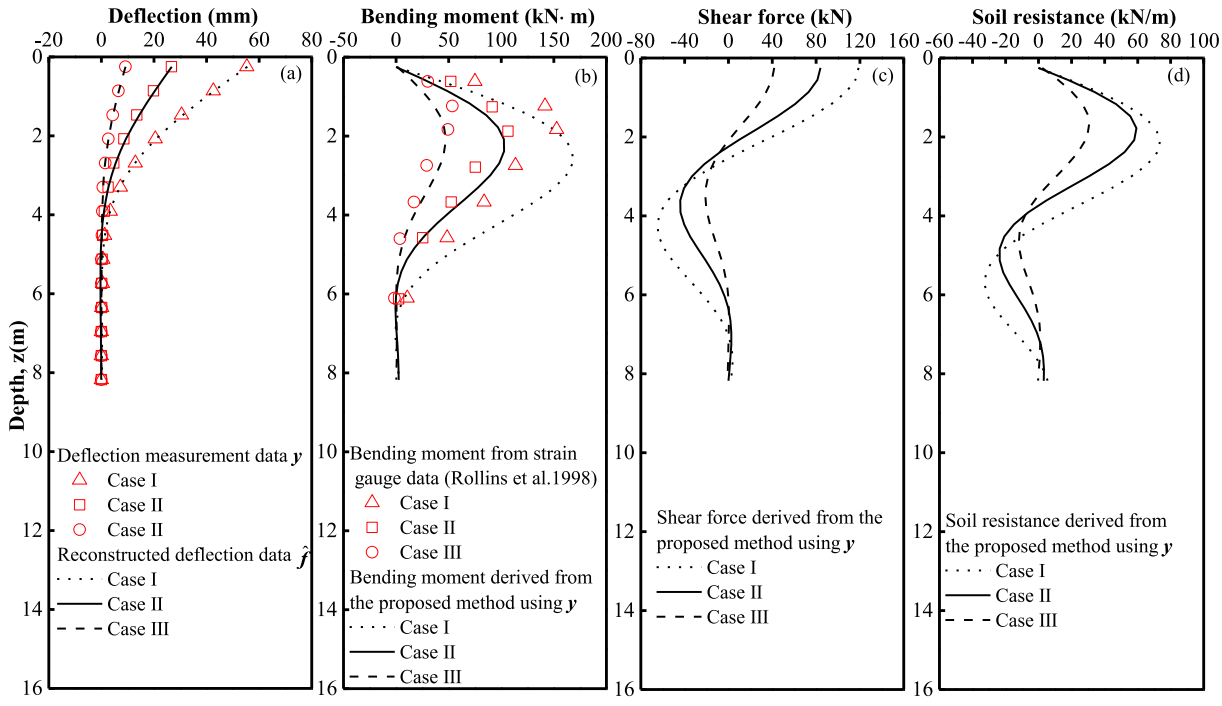

Fig. 4. Deflection data and interpreted results for front row of piles.

which is shown in Fig. 4(a) by a solid line. It can be observed that the solid line and the open squares almost overlap each other. It should be noted that there are only 14 original deflection measurement data points, while there are 27 reconstructed deflection measurement data points. In other words, the deflection data at locations where no deflections were taken can also be obtained using the proposed method. Fig. 4(b) plots the derived distribution of bending moments M from $\boldsymbol{y}$ along depth by a solid line. For comparison, Fig. 4(b) also includes the bending moments derived from the strain gauge data by Rollins et al. (1998) by open squares. It can be observed that the solid line is consistent with the open squares. Fig. 4(c) and (d) plot the derived distributions of shear force V and soil reaction p, respectively, from $\boldsymbol{y}$ along depth using solid lines.

Following the same procedure as that illustrated for Case II for the front row, the deflection measurement data for Cases I and III for the front row are represented and reconstructed in a similar manner, and are plotted by dotted and dashed lines, respectively, in Fig. 4(a), respectively. Fig. 4(a) shows that the dotted line almost overlaps the open triangles, and a similar observation can also be made between the dashed line and the open circles. The distributions of bending moments along depth are also derived from the measured defection data, following the procedure illustrated for Case II. Fig. 4(b) plots the distribution of bending moments for Cases I and III using the same symbols as those shown in Fig. 4(a). Fig. 4(b) also includes the distribution of bending moments derived from the strain gauge data by Rollins et al. (1998) for these two cases using the same symbols as those in Fig. 4(a). Fig. 4(b) shows that the bending moment distribution interpreted from the proposed method using deflection measurement data first increases with depth and then decreases with depth. This variation trend for the bending moments with depth from the proposed method is quite consistent with that derived from the strain gauge data, although there are some differences in the magnitudes of the bending moments. Fig. 4(c) and (d) also plot the derived distribution of shear forces and soil resistance, respectively, for the two cases, using the same symbols as those used in Fig. 4(a) and (b). $EI = (EI)_{\text{steel pipe}} + (EI)_{\text{concrete infill}}$, and the moment of inertia of the concrete was computed using ACI-318-95 (ACI, 1995) to account for the cracking of the concrete, which is consistent with Rollins et al. (1998).

For further testing, the proposed approach is also applied to derive the distributions of bending moments, shear forces, and soil resistance along depth for the middle and back rows under different loads, i.e., Cases I, II, and III. The results are summarized in Figs. 5 and 6 for the middle and back rows, respectively. It should be noted that both Figs. 5 and 6 contain four subplots: subplot (a) for deflection, subplot (b) for bending moments, subplot (c) for shear forces, and subplot (d) for soil resistance. Similar to Fig. 4(a), the reconstructed deflection data in Figs. 5(a) and 6(a) almost overlap the deflection measurement data. Furthermore, Figs. 5(b) and 6(b) show that the bending moments interpreted from the proposed method using deflection measurement data first increase with depth and then decrease with depth. The variation trend for the bending moments with depth is similar to that derived from the strain gauge data by Rollins et al. (1998), although there are some differences in the magnitudes of the bending

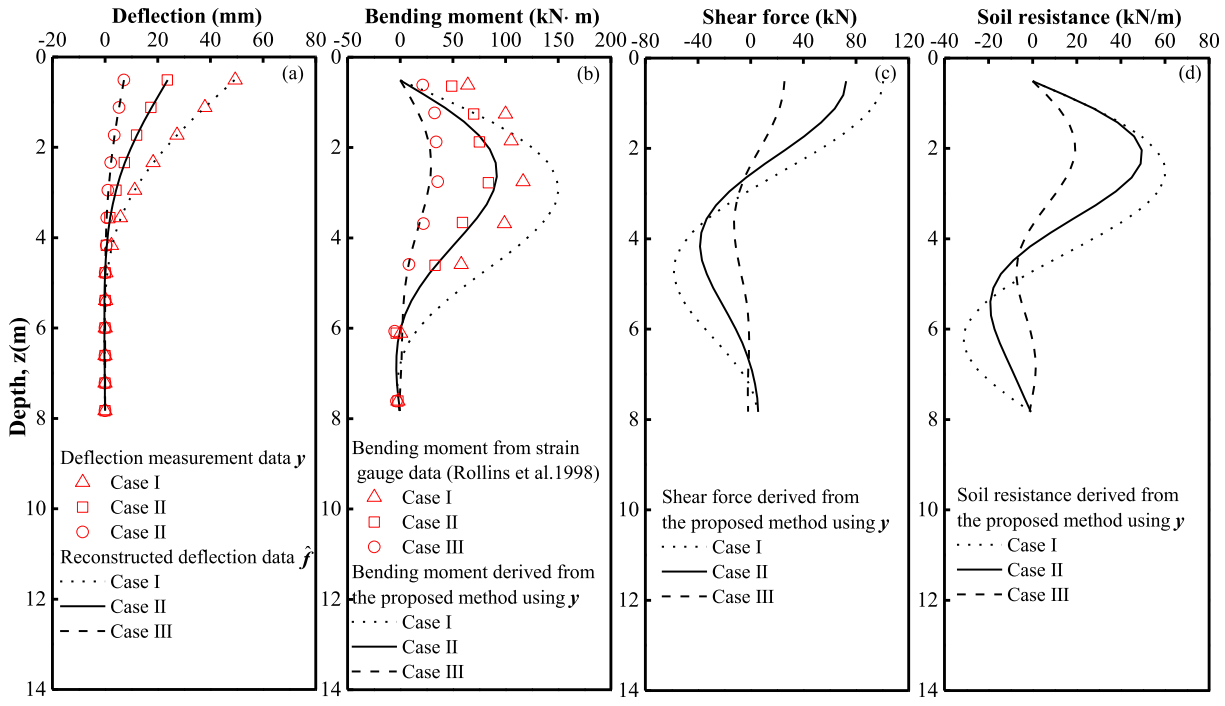

Fig. 5. Deflection data and interpreted results for middle row of piles.

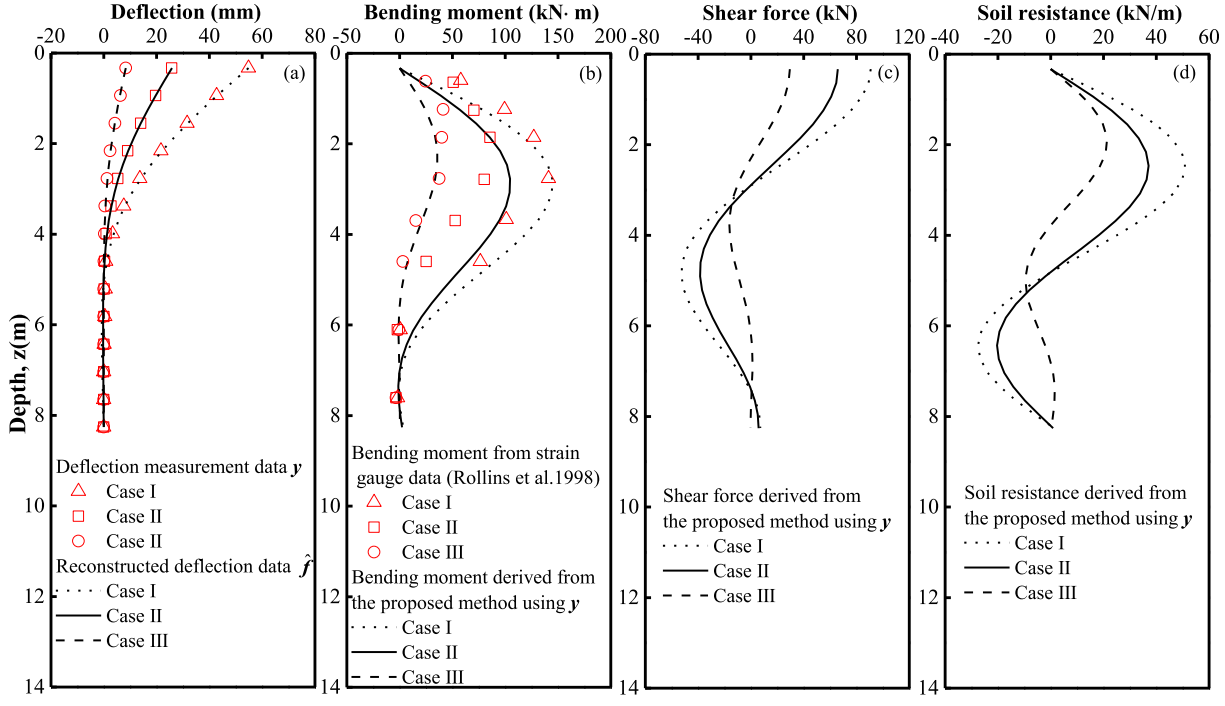

Fig. 6. Deflection data and interpreted results for back row of piles.

moments among each other. These agreements further demonstrate that the proposed method can properly reproduce the measured data and provide a reasonable interpretation of the bending moments. In addition, the shear forces and the soil resistance are also obtained as shown in Figs. 5(c) and (d) and 6(c) and (d) for piles in the middle and back rows, respectively. It should be noted that no results are shown at $z = 0$ m in Figs. 4–6, due to the interpolation nature of the proposed method in this study, as was discussed in Section 3.2.

Using the results shown in Figs. 4–6, further analysis can be performed. For example, the p-y curves at different depths, such as 1.0 m and 2.5 m, can be obtained using Figs. 4–6. Consider, for example, the p-y curve for the front

row of piles. Three different loading cases (i.e., Cases I, II, and III) are presented in Fig. 4. Fig. 4(a) plots the three sets of deflection measurement data corresponding to Cases I, II, and III. For each case, the deflection measurement data are reconstructed (as shown in Fig. 4(a)) and the distribution of soil resistance p (shown in Fig. 4(d)) is derived from that set of deflection measurement data. Therefore, there are three (p, y) data pairs at each depth, namely, 1.0 m and 2.5 m. "y" herein refers to the reconstructed deflection measurement data. Using the three (p, y) data pairs at a specific depth together with the origin point (0, 0), p-y curves for the front row at depths of 1.0 m and 2.5 m can be obtained, as shown in Fig. 7 by solid lines with open squares and with open triangles, respectively. Following the same procedure, p-y curves for the middle and back rows at depths of 1.0 m and 2.5 m can also be obtained from Figs. 5 and 6, respectively, as shown in Fig. 7. It is observed in Fig. 7 that the front row of piles carries the highest soil resistance (for both depths of 1.0 m and 2.5 m) and the middle row of piles carries slightly greater soil resistance than that of the back row of piles. These observations are generally consistent with those shown in previous studies (e.g., Rollins et al., 1998; Lin and Liao, 2006), although the proposed method predicts relatively lower and higher levels of soil resistance at depths of 1.0 m and 2.5 m, respectively, than those shown in Lin et al. (2005). Furthermore, a careful examination of Figs. 4(b)–6(b) shows that the depth to the maximum bending moment decreases as the soil resistance applied to the piles increases. The maximum bending moments occur at depths of around 2.7 m, 3.0 m, and 3.3 m for the front, middle, and back rows, respectively. This observation is also consistent with Rollins et al. (1998). All these agreements show that the proposed approach provides a reasonable interpretation of the lateral response of piles using the deflection measurement data.

As mentioned above, there are some differences in the magnitudes of the bending moments between those from the strain gauge data and those interpreted from the proposed method using inclinometer data (see Figs. 4(b)–6(b)). These differences in the magnitudes of bending moments may be attributed to: (1) the deflection measurement data containing measurement errors, (2) the strain gauge data also containing measurement errors, and the bending moments calculated from the strain gauge data also containing measurement errors; and (3) the deflection measurement data provided by Rollins et al. (1998) starting from depths of around 0.25 m, 0.51 m, and 0.33 m, as shown in Figs. 4–6, respectively. These points become inflection points when the measurement data are converted to periodic data in the proposed method (see the "periodic data" in Fig. 2), and the second-order derivatives (i.e., bending moment) at the inflection points are zero. Therefore, the bending moments obtained from the proposed method at depths of around 0.25 m, 0.51 m, and 0.33 m are zero. The obtained bending moments (i.e., the bending moments are zero at depths of around 0.25 m, 0.51 m, and 0.33 m, respectively) can be further improved, if displacement data above the ground surface are available from other sources, such as the linearly variable differential transducer (LVDT). In such cases, the displacement measurement data above the ground surface can be used together with the deflection measurement data below the ground surface to interpolate the deflection at the ground level. Then, the deflection obtained at the ground level can be used together with the deflection data obtained from the inclinometers to perform an analysis using the method proposed in this study. Unfortunately, although Rollins et al. (1998) mentioned that the LVDT was used to measure the displacement at an elevation of 0.3 m above the loading point, no data were reported in their paper. Therefore, the displacement data above the loading point cannot be used here to further improve the results shown in Figs. 4–6. The above discussions also imply that the proposed method is ideal for free-head piles with deflection measurements starting from the pile head (i.e., the loading level), but less suitable for other cases. This is a limitation of the proposed method. To illustrate and systematically test the proposed method, an LPILE demonstration example is adopted in the next section. For the LPILE example, (1) the deflection data are generated by the LPILE and free of measurement errors, (2) the bending moment and other lateral responses of the piles are calculated by the LPILE and free of measurement errors caused by the strain gauge data, and (3) the deflection data start at the loading level (e.g., ground surface).

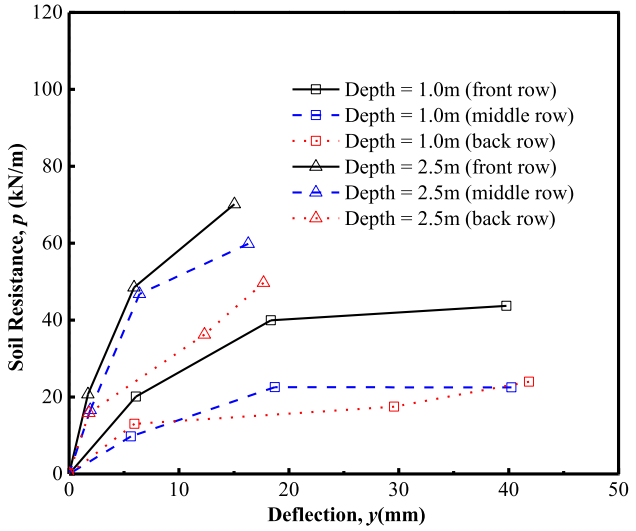

Fig. 7. Deduced p-y curves at depths of 1.0 m and 2.5 m.

5. Sensitivity study

The proposed method is further illustrated with a demonstration example used in the LPILE package (Ensoft, 2015) in this section. The deflection, soil conditions, and information on the piles are given by the software LPILE (Ensoft, 2015). Fig. 8 illustrates the configuration of this example. It consists of two soil layers.

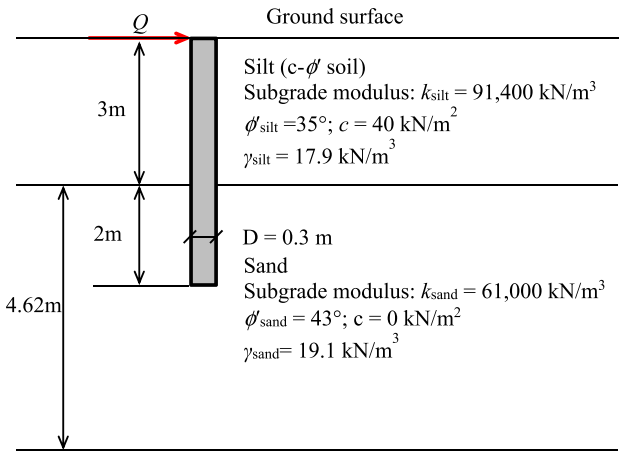

Fig. 8. Illustration of demonstration example used in LPILE (after Ensoft, 2015).

The first layer is a silt layer extending from the ground surface to a depth of 3 m, with a friction angle of $\phi'_{silt} = 35°$, undrained cohesion of $c = 40$ kN/m^2, an effective unit weight of $\gamma_{silt} = 17.9$ kN/m^3, a subgrade modulus of $k_{silt} = 91{,}400$ kN/m^3, and a strain factor of $\varepsilon_{50} = 0.005$. The second layer is a sand layer with a thickness of 4.62 m, a friction angle of $\phi'_{sand} = 43°$, an effective unit weight of $\gamma_{sand} = 19.1$ kN/m^3, and a subgrade modulus of $k_{sand} = 61{,}000$ kN/m^3. The pile in this demonstration example is a 5-m-long steel pile, with a diameter of $D = 0.3$ m, a modulus of elasticity of $E = 50.8$ GPa, and a moment of inertia of $I = 3.98 \times 10^{-4}$ m^4. The steel pile is subjected to a lateral load of $Q = 140.0$ kN, applied to the pile head, which is at the ground surface, as shown in Fig. 8. Using the above information and built-in p-y relations in the LPILE, the deflection of piles, the bending moment, the shear force, and the soil resistance with an interval of 0.05 m can be obtained. For the silt layer, a "silt (cemented c-phi)" p-y relation was selected, while a "Reese" p-y relation was adopted in the demonstration example. Detailed information can be found in Ensoft (2015). Since an interval of 0.05 m is adopted, there are 101 (5/0.05 + 1 = 101) data points in the deflection data. It should be noted that only part of the deflection data from this demonstration example will be taken as the "deflection measurement data" in this section to further illustrate the proposed method. It should be clarified that the bending moment, the shear force, and the soil resistance are also obtained from this demonstration example; they will be used for comparison purposes only.

5.1. Deflection data measured with equal intervals

Fig. 9(a) plots 21 deflection measurement data points with equal intervals of 0.25 m by open triangles. For a fair comparison, a resolution of interest of $\eta = 0.05$ m is specified. Following the procedure illustrated in the previous section, the deflection measurement data can be represented by a linear function and a set of orthogonal cosine functions. The reconstructed deflection data are plotted in Fig. 9(a) by a dashed line. Although only 21 deflection data points are measured here, the reconstructed ones have a length of 101, which is exactly the same as the original deflection data from the LPILE. Fig. 9(a) also includes the original deflection data from the LPILE by a solid line. It shows that the dashed line almost completely overlaps

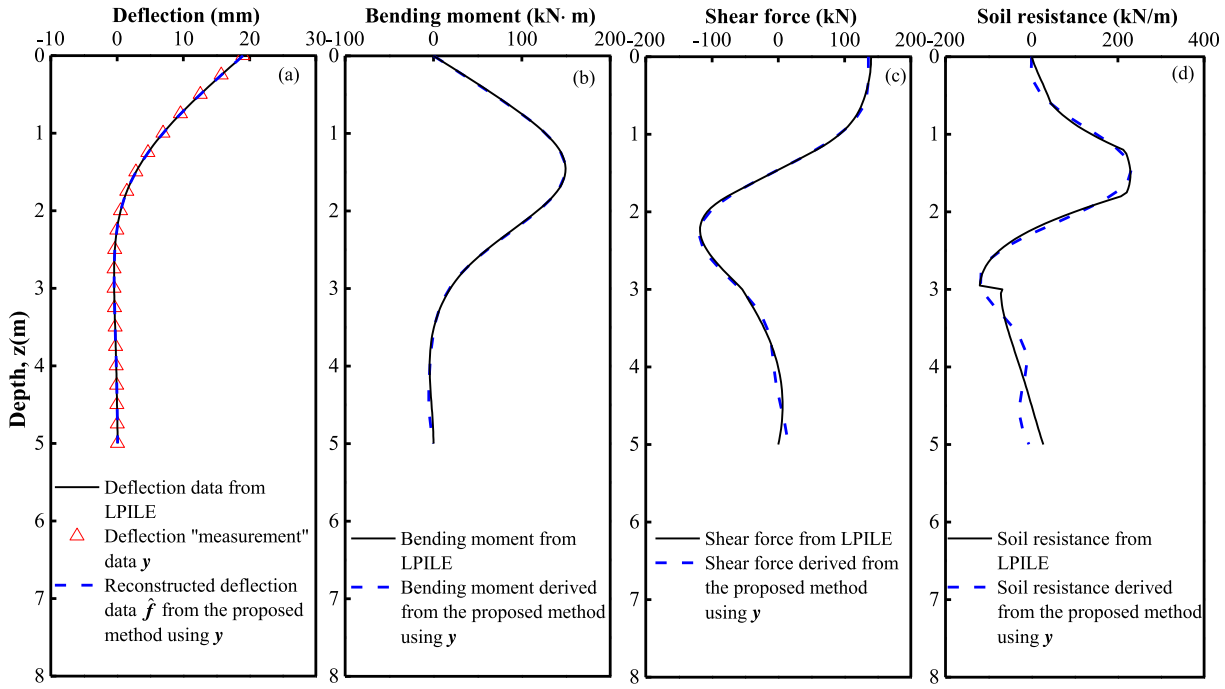

Fig. 9. Deflection data measured with equal intervals and interpreted results.

the open triangles and the solid line. This observation suggests that the deflection measurement data can be represented accurately by the proposed method, even at locations where no deflection data have been taken.

As the deflection measurement data are represented explicitly by a linear function and a set of orthogonal cosine functions, the derivatives of the deflection data with respect to depth can be obtained analytically, as shown in Eqs. (10)–(12). Substituting the obtained second-, third-, and fourth-order derivatives of the deflection data with respect to depth to Eqs. (1)–(3) leads to the distribution of bending moments, shear forces, and soil resistance, as shown in Eqs. (14)–(16). The bending moments, shear forces, and soil resistance derived from the deflection measurement data by the proposed method are shown in Fig. 9(b)–(d), respectively, by dashed lines. For comparison, Fig. 9(b)–(d) plot the original bending moments, shear forces, and soil resistance, respectively, from the LPILE by solid lines. It can be seen that those dashed lines are all in good agreement with the solid lines, although there are slight differences among them. It should be noted that only $K = 21$ deflection measurement data are used as input, while the derived lateral responses all have 101 data points. The consistency between the dashed lines and the solid lines suggests that the pile lateral response can be reasonably and accurately derived from the deflection measurement data, even at locations where no deflection data have been taken.

5.2. Deflection data measured with unequal intervals

For further illustration, the proposed method is used to derive the lateral response of piles when the deflection measurement data are taken with unequal intervals. For example, Fig. 10(a) plots 21 deflection measurement data points with unequal intervals by open triangles. Then, this set of measured deflection data is represented by a linear function and a set of orthogonal cosine functions using the proposed method in this study. The reconstructed deflection data are represented by a dashed line in Fig. 10(a). For comparison, Fig. 10(a) also includes the original deflection data from the LPILE by a solid line. It shows that the dashed line almost overlaps the solid line, which is similar to the observation shown in Fig. 9(a). This again demonstrates that the proposed method can accurately reproduce the deflection measurement data even at locations where no deflection data have been taken. Then, following the same procedure illustrated previously, the distribution of bending moments, shear forces, and soil resistance along depth can also be obtained, as shown in Fig. 10(b)–(d), respectively, by dashed lines. Similar to Fig. 9(b)–(d), Fig. 10 (b)–(d) also plot the original bending moments, shear forces, and soil resistance from the LPILE by solid lines. Observations similar to those shown in Fig. 9(b) and (d) can also be obtained; the dashed lines agree quite well with the solid lines. This suggests that the pile lateral response can be properly derived from the deflection measurement data with unequal intervals by the proposed method.

5.3. Effect of pre-processing

It should be noted that all the previous scenarios utilized the pre-processing technique described in Section 3.2 entitled "Pre-processing of deflection measurement data". The effect of pre-processing is illustrated in this subsection

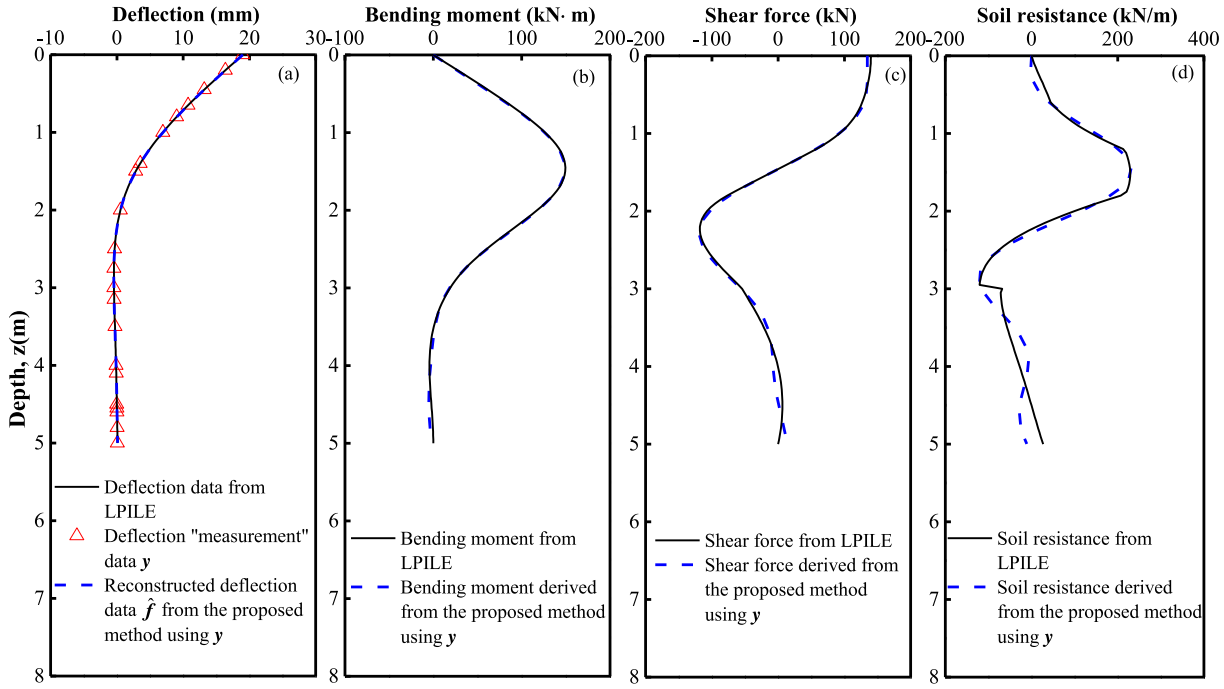

Fig. 10. Deflection data measured with unequal intervals and interpreted results.

by comparing the results with and without the use of pre-processing. Consider, for example, the deflection data shown in Fig. 9(a) by open triangles. First, this set of deflection measurement data is used directly by the proposed method. Namely, the OMP algorithm is performed directly to reconstruct the deflection measurement data, and no decomposition shown in Fig. 1 or the transformation shown in Fig. 2 (i.e., $L_P = 0$) is used. To be consistent with the demonstration example from the LPILE, the same resolution of $\eta = 0.05$ m is still used here. As this set of deflection data is represented by a set of orthogonal cosine functions, derivatives can be readily obtained. Substituting the obtained derivatives into Eqs. (1)–(3) leads to the distribution of bending moments, shear forces, and soil resistance along depth. Fig. 11(a)–(d) plot the reconstructed deflection data (without using pre-processing), the derived distribution of bending moments, shear forces, and soil resistance, respectively, by dotted lines with crosses. For comparison, Fig. 11(a)–(d) also include the original deflection, bending moments, shear forces, and soil resistance from the LPILE by solid lines. It can be clearly observed in Fig. 11(a) that the dotted line with crosses is in relatively good agreement with the open triangles and the solid line. This suggests that that pre-processing has little effect on the reconstruction of the deflection measurement data. However, the high-order derivatives of the deflection measurement data, and hence, the lateral response of piles, are significantly affected by pre-processing. As shown in Fig. 11(b)–(d), the lateral response of the piles derived from the deflection measurement data (without using pre-processing) deviates significantly from the original one derived from the LPILE.

In contrast, if pre-processing is used to deal with the deflection measurement data, as illustrated in Figs. 1 and 2, the results are significantly improved, particularly for the interpreted lateral response. Note that the procedure in Fig. 2 involves transforming the nonlinear component of the deflection data into a periodic signal by alternately cloning it and its folded and inverted copies along the depth coordinate for L_P times. Different L_P (e.g., $L_P = 9$, 17, and 19) may lead to different results. Fig. 11 also plots the results corresponding to different L_P scenarios, i.e., $L_P = 9$, 17, and 19, by solid lines with open circles, squares, and stars, respectively. Fig. 11(a) suggests that the reconstructed deflection measurement data for all the L_P scenarios are in good agreement with the original one from the LPILE, as expected. However, the derived lateral responses for the different L_P values are quite different; the derived lateral response of the pile becomes more and more consistent with the original lateral response from the LPILE as the L_P increases from 0 to 19. As L_P increases, the predicted results tend to approach a constant result, which can be observed for the $L_P = 17$ and 19 scenarios in Fig. 11. It is seen that the results (i.e., the solid lines with squares ($L_P = 17$ scenario) and the solid line with stars ($L_P = 19$ scenario)) almost overlap each other. This observation is used to determine the L_P value when employing the proposed method in this study. In other words, L_P is increased in the proposed method until the pile lateral response

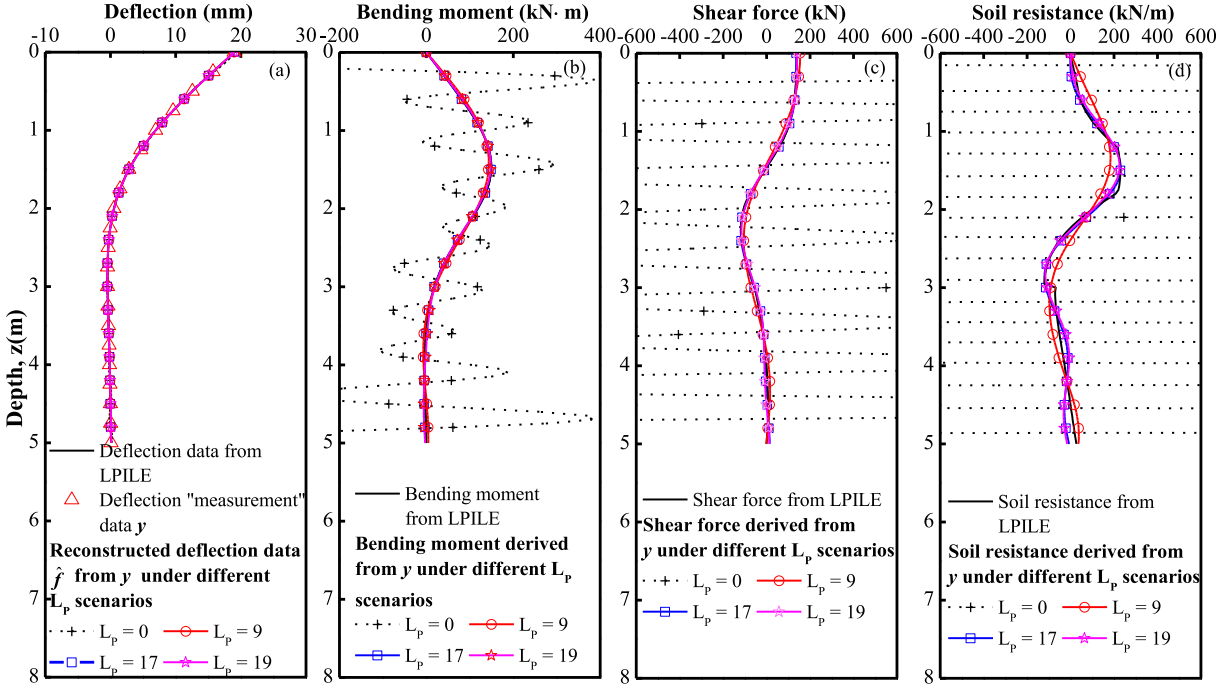

Fig. 11. Effect of pre-processing technique.

obtained from the proposed method remains unchanged. In summary, when compared to the results without using pre-processing, the interpreted lateral response of piles using pre-processing is more reasonable.

In addition, it is worth noting that the proposed method is applicable to short piles, which have also been tested in the sensitivity study, although only the long piles cases are reported in this paper due to page limitations.

6. Summary and conclusion

This paper proposed a novel approach to interpreting the lateral response of piles/drilled shafts from discrete deflection measurement data. The proposed method was based on compressive sampling (CS), and it only requires discrete deflection measurement data versus depth and flexural rigidity as input, while it provides the lateral response, such as the distribution of bending moments, shear forces, and soil resistance along depth in an almost continuous manner as output. In other words, the proposed method can be used to derive the lateral response even at locations where no deflection data have been measured. Moreover, the deflection measurement data can be used with either equal or unequal intervals. During the implementation of the proposed method, the deflection measurement data were decomposed into linear and nonlinear components. The linear component was represented by a linear function, while the nonlinear component was transformed into a periodic data set, which significantly improved the interpretation of the lateral response.

Equations were derived for the proposed method. A real case history from a full-scale laterally loaded pile test in the USA and a sensitivity study were used to illustrate and validate the proposed method. The results in the real case study showed that the proposed method provides an accurate reconstruction of the deflection profile and a reasonable interpretation of the lateral response of piles/drilled shafts. The proposed method is ideal for free-head piles with deflection measurements starting from the pile head (i.e., the loading level), but less suitable for other cases. On the other hand, the results of the sensitivity study further showed that the proposed method in this study is robust and accurate. In addition, the effect of the proposed pre-processing method was explored in the sensitivity study.

Acknowledgements

The authors would like to thank the anonymous reviewers for their valuable comments and constructive suggestions which significantly improved the quality of the manuscript. The work described in this paper was supported by grants from the Research Grants Council of the Hong Kong Special Administrative Region, China (Project No. 9042172 (CityU 11200115) and Project No. 9042516 (CityU 11213117)). The financial support is gratefully acknowledged.

References

American Concrete Institute, 1995. ACI building code requirements for structural 18 concrete and commentary. ACI 318-95, Farmington Hills, Michigan, USA.

Boggess, A., Narcowich, F.J., 2009. A First Course in Wavelets with Fourier Analysis. Wiley, New Jersey, USA, pp. 235–236.

Brandenberg, S., Wilson, D., Rashid, M., 2010. Weighted residual numerical differentiation algorithm applied to experimental bending moment data. J. Geotech. Geoenviron. Eng. https://doi.org/10.1061/(ASCE)GT.1943-5606.0000277, 854-863.

Brown, D.A., Hidden, S.A., Zhang, S., 1994. Determination of *p-y* curves using inclinometer data. Geotech. Test. J. 17 (2), 150–158.

Candès, E.J., Romberg, J.K., Tao, T., 2006. Stable signal recovery from incomplete and inaccurate measurements. Commun. Pure Appl. Math. 59 (8), 1207–1223.

Candès, E.J., Wakin, M.B., 2008. An introduction to compressive sampling. IEEE Signal Proc. Mag. 25 (2), 21–30.

Chien, C.J., Lin, S.S., Yang, C.C., Liao, J.C., 2013. Lateral performance of drilled shafts due to combined lateral and axial loading. J. Mech. 29 (4), 685–693.

Das, B.M., 2015. Principles of Foundation Engineering. Cengage learning, Stamford, Connecticut, USA.

Daubechies, I., 1992. Ten Lectures on Wavelets. Society for Industrial and Applied Mathematics.

Donoho, D.L., 2006. Compressed sensing. IEEE Trans. Inf. Theory 52 (4), 1289–1306.

Ensoft, 2015. LPILE v8.0 – A Program for the Analysis and Design of Piles and Drilled Shafts under Lateral Loads.

Foucart, S., Rauhut, H., 2013. A Mathematical Introduction to Compressive Sensing. Birkhäuser, Boston.

Gu, L.L., Ye, G.L., Bao, X.H., Zhang, F., 2016. Mechanical behaviour of piled-raft foundations subjected to high-speed train loading. Soils Found. 56 (6), 1035–1054.

Gupta, B.K., Basu, D., 2017. Analysis of laterally loaded short and long piles in multilayered heterogeneous elastic soil. Soils Found. 57 (1), 92–110.

Hardy, G.H., 2000. In: Divergent Series, vol. 334. American Mathematical Society, New York, USA.

Hassiotis, S., Chameau, J., Gunaratne, M., 1997. Design method for stabilization of slopes with piles. J. Geotech. Geoenviron. Eng. 123 (4), 314–323.

Hetenyi, M., 1946. Beams on Elastic Foundation: Theory with Applications in the Fields of Civil and Mechanical Engineering. University of Michigan, Ann Arbor.

Huang, Y., Beck, J.L., Wu, S., Li, H., 2014. Robust Bayesian compressive sensing for signals in structural health monitoring. Comput-aid. Civ. Inf. 29 (3), 160–179.

Karthigeyan, S., Ramakrishna, V.V.G.S.T., Rajagopal, K., 2007. Numerical investigation of the effect of vertical load on the lateral response of piles. J. Geotech. Geoenviron. Eng. 133 (5), 512–521.

Kourkoulis, R., Gelagoti, F., Anastasopoulos, I., Gazetas, G., 2011. Slope stabilizing piles and pile-groups: parametric study and design insights. J. Geotech. Geoenviron. Eng. https://doi.org/10.1061/(ASCE)GT.1943-5606.0000479, 663-677.

Kourkoulis, R., Gelagoti, F., Anastasopoulos, I., Gazetas, G., 2012. Hybrid method for analysis and design of slope stabilizing piles. J. Geotech. Geoenviron. Eng. 138 (1), 1–14.

Li, X.S., Yang, J., Liu, H., 1998. Differentiation of noisy experimental data for interpretation of nonlinear stress-strain behavior. J. Eng. Mech. 124 (7), 705–712.

Lin, S.S., Liao, J.C., Chen, J.T., Chen, L., 2005. Lateral performance of piles evaluated via inclinometer data. Comput. Geotech. 32 (6), 411–421.

Lin, S., Liao, J., 2006. Lateral response evaluation of single piles using inclinometer data. J. Geotech. Geoenviron. Eng. 132 (12), 1566–1573.

Lin, S., Lai, C.H., Chen, C.H., Ueng, T.S., 2010. Derivation of cyclic p-y curves from instrumented dynamic lateral load tests. J. Mech. 26 (2), 123–133.

Mallat, S., 1999. A Wavelet Tour of Signal Processing. Academic Press, New York, USA.
Martin, G.R., Chen, C.Y., 2005. Response of piles due to lateral slope movement. Comput. Struct. 83 (8–9), 588–598.
Mathworks, Inc. 2017. MATLAB — The Language of Technical Computing. (Accessed on March 21, 2017). (http://www.mathworks.com/products/matlab/).
McClelland, B., Focht, J., 1958. Soil modulus for laterally loaded piles. Trans. ASCE 123, 1049–1086.
Motamed, R., Sesov, V., Towhata, I., Anh, N.T., 2010. Experimental modeling of large pile groups in sloping ground subjected to liquefaction-induced lateral flow: 1-G shaking table tests. Soils Found. 50 (2), 261–279.
Ooi, P.S.K., Ramsey, T.L., 2003. Curvature and bending moments from inclinometer data. Int. J. Geomech. 3 (1), 64–74.
Oppenheim, A.V., Schafer, R.W., 1989. Discrete-Time Signal Processing. Prentice Hall Inc, Englewood Cliffs, New Jersey, USA.
Poulos, H.G., 1995. Design of reinforcing piles to increase slope stability. Can. Geotech. J. 32 (5), 808–818.
Pati, Y.C., Rezaiifar, R., Krishnaprasad, P.S., 1993. Orthogonal matching pursuit: recursive function approximation with applications to wavelet decomposition. Proceedings of 27th Asilomar Conference on Signals Systems and Computers. Pacific Grove, Calif., 1–3 November 1993. IEEE, New York, pp. 40–44.
Reese, L.C., Van Impe, W.F., 2001. Single Piles and Pile Groups under Lateral Loading. CRC Press, Rotterdam, Netherlands, pp. 121–123.
Rollins, K., Peterson, K., Weaver, T., 1998. Lateral load behavior of full-scale pile group in clay. J. Geotech. Geoenviron. Eng. 124 (6), 468–478.
Salomon, D., 2004. Data Compression: The Complete Reference. Springer Science and Business Media, New York.
Smith, M.J., Eddins, S.L., 1990. Analysis/synthesis techniques for subband image coding. IEEE Trans. Acoust. Speech, Signal Process. 38 (8), 1446–1456.
Sun, S.W., Zhu, B.Z., Wang, J.C., 2013. Design method for stabilization of earth slopes with micropiles. Soils Found. 53 (4), 487–497.
Tropp, J.A., Gilbert, A.C., 2007. Signal recovery from random measurements via orthogonal matching pursuit. IEEE Trans. Inf. Theory 53 (12), 4655–4666.
Wang, S.T., Reese, L.C., 1991. Analysis of Piles Under Lateral Load-Computer Program COM624P for the Microcomputers. U.S. Dept. of Transportation, FHWA, Washington, D.C., Report No. FHWA-SA-91-002.
Wang, Y., O'Rourke, T.D., 2007. Interpretation of secant shear modulus degradation characteristics from pressuremeter tests. J. Geotech. Geoenviron. Eng. 133 (12), 1556–1566.
Wang, Y., Akeju, O.V., Zhao, T., 2017. Interpolation of spatially varying but sparsely measured geo-data: a comparative study. Eng. Geol. 231, 200–217.
Wang, Y., Zhao, T., Phoon, K.K., 2018. Direct simulation of random field samples from sparsely measured geotechnical data with consideration of uncertainty in interpretation. Can. Geotech. J. 55 (6), 862–880.
Wang, Y., Zhao, T., 2016. Interpretation of soil property profile from limited measurement data: a compressive Sampling perspective. Can. Geotech. J. 53 (9), 1547–1559.
Wang, Y., Zhao, T., 2017. Statistical interpretation of soil property profiles from sparse data using Bayesian Compressive Sampling. Géotechnique 67 (6), 523–536.
Wilson, D.W., 1998. Soil-pile-Superstructure Interaction in Liquefying Sand and Soft Clay (Ph.D Thesis). University of California at Davis.
Wilson, D., Boulanger, R., Kutter, B., 2000. Observed seismic lateral resistance of liquefying sand. J. Geotech. Geoenviron. Eng. 126 (10), 898–906.
Yamin, M.M., Liang, R.Y., 2010. Interpreting the behavior of laterally loaded drilled shaft from measured deflection data. Int. J. Numer. Anal. Met. 34 (8), 859–877.
Yang, Z., Jeremić, B., 2002. Numerical analysis of pile behaviour under lateral loads in layered elastic–plastic soils. Int. J. Numer. Anal. Methods Geomech. 26 (14), 1385–1406.
Zhao, T., Montoya-Noguera, S., Phoon, K.K., Wang, Y., 2018. Interpolating spatially varying soil property values from sparse data for facilitating characteristic value selection. Can. Geotech. J. 55 (2), 171–181.
Zhao, T., Wang, Y., 2018. Simulation of cross-correlated random field samples from sparse measurements using Bayesian compressive sensing. Mech. Syst. Signal Process. 112, 384–400.